

# The Incidence of Debris Disks at 24 $\mu\text{m}$ and 670 Myr

Laurie E. Urban<sup>1,2</sup>, George Rieke<sup>3</sup>, Kate Su<sup>3</sup>, David E. Trilling<sup>1</sup>

## ABSTRACT

We use *Spitzer Space Telescope* 24  $\mu\text{m}$  data to search for debris disks among 122 AFGKM stars from the  $\sim 670$  Myr clusters Hyades, Coma Ber, and Praesepe, utilizing a number of advances in data reduction and determining the intrinsic colors of main sequence stars. For our sample, the  $1\sigma$  dispersion about the main sequence V- $K_S$ ,  $K_S$ -[24] locus is approximately 3.1%. We identify seven debris disks at 10% or more ( $\geq 3\sigma$  confidence level) above the expected  $K_S$  - [24] for purely photospheric emission. The incidence of excesses of 10% or greater in our sample at this age is  $5.7^{+3.1}_{-1.7}\%$ . Combining with results from the literature, the rate is  $7.8^{+4.2}_{-2.1}\%$  for early-type (B9 - F4) stars and  $2.7^{+3.3}_{-1.7}\%$  for solar-like (F5 - K9) stars. Our primary sample has strict criteria for inclusion to allow comparison with other work; when we relax these criteria, three additional debris disks are detected. They are all around stars of solar-like type and hence reinforce our conclusion that disks around such stars are still relatively common at 670 Myr and are similar to the rate around early-type stars. The apparently small difference in decay rates between early-type and solar-like stars is inconsistent with the first order theoretical predictions that the later type stellar disks would decay an order of magnitude more quickly than the earlier type ones.

*Subject headings:* circumstellar disks — infrared: stars — open clusters: Hyades, Coma Ber, Praesepe

## 1. Introduction

Most stars form with an accompanying protoplanetary disk. Initially these disks begin as dense optically thick regions mostly made up of primordial gas and dust; these constituents make the disks readily detectable in thermal continuum and multiple emission lines. These disks provide the environment for massive planet formation. Ironically, once planets have formed the disks

---

<sup>1</sup>Department of Physics and Astronomy, Northern Arizona University, P.O. Box 6010, Flagstaff, AZ 86011, USA

<sup>2</sup>Institute for Astronomy, University of Hawaii at Manoa, 2680 Woodlawn Dr, Honolulu, HI 96822, USA

<sup>3</sup>Steward Observatory, University of Arizona, Tucson, AZ 85721, USA

disappear after a few million years (e.g., Haisch et al. 2001). The resulting planetary systems remain difficult to detect directly. The systems have not ceased evolving at this point; terrestrial planets continue to grow from the solid remnants of the disks (e.g., Agnor, Canup & Levison 1990; Chambers 2001; Raymond et al. 2006; Morishima et al. 2010), and massive planets may migrate inward or outward (Hahn & Malhotra 1999; Gomes, Morbidelli & Levison 2004; Levison et al. 2007). These processes are marked by dynamical stirring of the asteroidal or planetesimal bodies, which are pulverized into dust that is warmed by the star and glows in the infrared. This dust dissipates rapidly due to radiation pressure, Poynting-Robertson drag, or collisional destruction (e.g., Lagrange et al. 2000; Dominik & Decin 2003). Hence, these debris disks must reflect the current state of the systems, and the infrared excesses provide snapshots of the state of the circumstellar material and of the degree of dynamical activity causing it to undergo collisions. A series of these snapshots gives a view of evolution of the planetary system (e.g., Kenyon & Bromley 2004; Wyatt 2008).

Debris disks were first observed in the infrared with the *Infrared Astronomical Satellite (IRAS)* (Aumann et al. 1984; see also Rhee et al. 2007). Many subsequent debris disk observations were made with the *Infrared Space Observatory (ISO)* (e.g., Decin et al. 2000; Spangler et al. 2001; Habing et al. 2001; Decin et al. 2003). The Multiband Imaging Photometer for *Spitzer* (MIPS; Rieke et al. 2004) on board the *Spitzer Space Telescope* provided another significant increase in sensitivity, observing a large number of debris disks at 24 and 70  $\mu\text{m}$ . *Herschel* is currently extending our understanding of large samples of debris disks to longer infrared and submillimeter wavelengths.

The evolution of the 24  $\mu\text{m}$  emission of debris disks is particularly interesting because this wavelength traces inner zones of these systems that may reveal processes near the ice line (Morales et al. 2011) and because the dynamical timescale for these zones is shorter than for those probed at longer wavelengths, so the evolution should proceed relatively rapidly. Previous surveys have verified that the 24  $\mu\text{m}$  emission of debris disks decays significantly over time. About 50% of early-type stars younger than 30 Myr have debris disks detected at 24  $\mu\text{m}$  (Rieke et al. 2005 and Su et al. 2006). However, at 100 to 115 Myr the detection rate has dropped to about 35% (see below). Gáspár et al. (2009) find the Praesepe cluster at  $\sim 750$  Myr to have an excess rate of only  $\sim 2\%$ . Surveys of stars older than  $\sim 1$  Gyr report an excess rate of  $\sim 4\%$  or less (Meyer et al. 2008, Trilling et al. 2008, Koerner et al. 2010).

A better understanding of the decay process will help build a picture of the evolution of planetary systems. Toward this goal, we examine MIPS data at 24  $\mu\text{m}$  for three stellar clusters with ages  $\sim 670$  Myr: Hyades ( $\sim 650$  Myr; Perryman et al. 1998, De Gennaro et al. 2009), Coma Ber ( $\sim 600$  Myr; Collier et al. 2009), and Praesepe ( $\sim 750$  Myr; Gáspár et al. 2009). We improve on previous studies by combining results for three separate clusters of similar ages. This study

also improves over similar work on field stars because the ages of our sample are much better constrained. Combining three clusters provides a high fidelity measurement over a large range of spectral types from early K for the closest cluster (Hyades) to A-types with reasonable statistics for the richest but most distant (Praesepe).

We discuss in Section 2 how we selected our sample for this study, reduced the data, excluded stars with large errors or bad measurements, and placed our retained targets on a  $V - K_S$  versus  $K_S - [24]$  color-color diagram (Gorlova et al. 2006). We improve on previous results by utilizing a new locus for the photospheres of main sequence stars. In Section 3 we determine which stars have excess emission at  $24 \mu\text{m}$  and compare our work with that of others. Section 4 discusses the excess rate at 670 Myr as a function of spectral type. We also compare these results to previously published excess rates and discuss the decay rate of  $24 \mu\text{m}$  excesses. Our conclusions are in Section 5.

## 2. Observations and Data Reduction

### 2.1. Sample Selection and Data Reduction

We searched the *Spitzer* archive for observations of stars in published membership lists for the Hyades, Coma Ber, and Praesepe. Our initial samples included 78 stars from the Hyades (Paulson et al. 2004), 84 from Coma Ber (Abad et al. 1999), and 193 from Praesepe (Gáspár et al. 2009). Some of the stars have accompanying  $70 \mu\text{m}$  observations; here we only report the  $24 \mu\text{m}$  results, some of which have been published previously (Rieke et al. 2005; Su et al. 2006; Cieza et al. 2008; Carpenter et al. 2008; Gáspár et al. 2009).

For consistency, we re-processed all the data as part of a *Spitzer* legacy catalog (Su et al. 2010), using the MIPS instrument team Data Analysis Tool (Gordon et al. 2005) for basic reduction. In addition, a second flat field constructed from the  $24 \mu\text{m}$  data itself was applied to all the  $24 \mu\text{m}$  results to remove scattered-light gradients and dark latency (e.g., Engelbracht et al. 2007). The processed data were then combined using the World Coordinate System (WCS) information to produce final mosaics with pixels half the size of the physical pixel scale. The majority of the stars in the Praesepe cluster were observed in scan-map mode as presented in Gáspár et al. (2009). We used the same data reduction as in that paper, but did the photometry differently as described below.

We extracted the photometry using PSF fitting. The input PSFs were constructed using observed calibration stars and smoothed STinyTim model PSFs, and have been tested to ensure the photometry results are consistent with the MIPS calibration (Engelbracht et al. 2007). Aperture photometry was also performed, but the results were only used as a reference to screen targets that

might have contamination from nearby sources or background nebulosity.

The random photometry errors were estimated based on the pixel-to-pixel variation within a  $2' \times 2'$  box centered on the source position. The final photometry errors also included the errors from the detector repeatability ( $\lesssim 1\%$  at  $24 \mu\text{m}$ , Engelbracht et al. 2007). The measured flux densities,  $24 \mu\text{m}$  magnitudes ([24], using 7.17 Jy as the zero magnitude flux; Rieke et al. 2008), and associated errors are listed in Table 1.

## 2.2. Culling the Sample

We further trimmed the sample based on the criteria described below to ensure our analysis only includes measurements of uniform quality. Because of *Spitzer's* exceptional pointing accuracy ( $< 1''$ ), we considered a source only where the PSF fitting position falls within  $1''.5$  of the member position (from the membership catalogs). Sources that failed this positional test are noted as “6” in Table 1. We then eliminated by visual inspection of the  $24 \mu\text{m}$  images all stars with a nearby source (within  $6''$ ) of the target star (noted as “1” in Table 1). We excluded all stars that are classified as giants (luminosity class III) (noted as “7” in Table 1). We also excluded all stars that could not be detected by eye, implying a signal to noise ratio  $< 3$  (noted as “3” in Table 1); this step guarded against false detections in regions where the background had residual structure. Finally, we excluded all measurements with a FWHM either much greater or less than the nominal FWHM of the MIPS beam of  $\sim 5''.5$  (noted as “2” in Table 1), which is an indication of confusion with a second object.

In our analysis we rely on  $K_S$  magnitudes from 2MASS (Cutri et al. 2003). For stars in the Hipparcos catalog (Perryman et al. 1997), we adopted the listed Johnson V photometry. For stars that are not in Hipparcos but are in Praesepe we adopted the V magnitudes gathered by Gáspár et al. (2009); we collected additional V magnitudes from the Simbad database. A total of 8 stars have no available V magnitudes, noted as “5” in Table 1; these stars are not included in our analysis.

Finally, we removed stars with large errors in  $K_S - [24]$ . (The errors from  $V - K_S$  are not used to remove stars from our sample since the errors in the V magnitudes are generally small and any stars with large errors in  $K_S$  will be eliminated because of the errors in  $K_S - [24]$ .) We took the  $K_S$  errors ( $e_{K_S}$ ) from 2MASS. For the MIPS photometry, we combined two types of error. The first,  $e_{24,pp}$ , is based on the pixel-to-pixel variation near the source and represents the random photometric error. The second arises from the overall repeatability of the MIPS  $24 \mu\text{m}$  measurement at  $\sim 1\%$  of the source fluxes (Engelbracht et al. 2007). The final error ( $e_{24}$ ) in the  $24 \mu\text{m}$  flux ( $f_{24}$ ) is thus

$$e_{24} = \sqrt{e_{24,pp}^2 + (0.01 * f_{24})^2}. \quad (1)$$

We combine the 24  $\mu\text{m}$  errors with the  $K_S$  errors to find the total (RMS) error on  $K_S - [24]$ . Only stars with  $e_{K_S-[24]} < 0.05$  were retained (exclusion note “4” in Table 1). Our final sample contains 122 stars: 61 from Hyades, 25 from Coma Ber, and 36 from Praesepe. We present all 355 stars in Table 1, where we indicate the 122 stars included and the reason the remaining were excluded from analysis.

### 2.3. Main Sequence Definition and Scatter

Figure 1 shows the  $V - K_S$  vs.  $K_S - [24]$  color-color plot for the whole sample, and the final sample retained in our analysis. Gorlova et al. (2006) introduced such a diagram to determine the photospheric locus for main sequence stars in the Pleiades cluster. They identified stars with infrared excesses as those with  $K_S - [24]$  positive by more than  $3\sigma$  relative to the photospheric locus. Here we apply the same general technique. We have used a sample of  $\sim 1300$  stars from the *Spitzer* archive (Su et al. 2010) to derive the locus of main sequence stars in  $V - K_S, K_S - [24]$  space. We define  $x = V - K_S - 0.8$ . For  $x \leq 0$ , we find the following empirical fits:

$$K_S - [24] = \frac{(50 + 661x + 282x^2 + 653x^3)}{10000}; \quad (2)$$

whereas for  $x > 0$ , we find:

$$K_S - [24] = \frac{(55 - 134x + 655.5x^2 - 1095x^3 + 664.15x^4 - 145.8x^5 + 11.01x^6 - 0.03x^7)}{10000}. \quad (3)$$

At the juncture where  $V - K_S = 0$  the equations agree so either of them applies. The RMS scatter around these fits (determined by fitting gaussians to the distribution so the result is not biased by stars with excesses) is 0.038 magnitudes.

Small color shifts in our clusters are possible due to effects such as metallicity differences or low levels of reddening (e.g., the probable reddening of Praesepe proposed by Taylor et al. (2006) translates to  $\sim 0.01$  mag at  $K_S$ ). We allowed the colors for each cluster to shift horizontally (in the  $K_S - [24]$  direction) to find the overall best fit to the ensemble of stars, with different shifts allowed for  $x \leq 0$  and  $x > 0$ . We found the horizontal offset for each cluster by minimizing the calculated  $\chi^2$ , defined as:

$$\chi^2 = \sum [(K_S - [24])_{\text{observed}} - (K_S - [24])_{\text{predicted}}]^2. \quad (4)$$

We did not want to skew the  $\chi^2$  values with the redder K and M stars; therefore, we chose an upper bound of  $V - K_S = 2.5$  for the  $\chi^2$  minimization. We included only a range between  $-0.1$  and  $0.1$  in  $K_S - [24]$  (i.e.,  $3\sigma$  in our fit) so that possible excess stars did not contaminate our results.

Table 2 gives shifted values for each of the clusters. We found a systematic offset of about 0.02 between the blue and red segments of the fit, which probably indicates a residual problem in our determination of the main sequence locus. The scatter improves to 0.031 mag after implementing these shifts (Figure 2).

### 3. Results

#### 3.1. Identification of stars with excess emission

We first identified excess candidates by requiring that the difference between the observed  $K_S - [24]$  and the predicted  $K_S - [24]$  is  $\gtrsim 0.1$  mag. There are nine stars that meet this criterion. To ensure the excess is significant, we also compute  $\chi_{24}$ , defined as

$$\chi_{24} = \frac{(K_S - [24])_{\text{observed}} - (K_S - [24])_{\text{predicted}}}{e_{K_S - [24]}}. \quad (5)$$

A significant excess requires  $\chi_{24} \geq 3$  (Su et al. 2006, Trilling et al. 2008). One of the nine stars, 2MASS J08385506+1911539, from the Praesepe cluster failed this test ( $\chi_{24} = 2.7$ ); we eliminated it from the list of confirmed excesses. We therefore find that eight out of our sample of 122 stars have excesses at 24  $\mu\text{m}$  greater than 10% of their photospheric emission and at a minimum  $3\sigma$  confidence level (Figure 3 and Table 3). Five of these eight stars have previously been identified as having 24  $\mu\text{m}$  excesses: HD 28226 and HD 28355 (Su et al. 2006, Cieza et al. 2008); 2MASS J08411840+1915394 (Gáspár et al. 2009); and HD 285690 and HD 286789 (Stauffer et al. 2010). The three stars with newly discovered excesses are HD 108382, HIP 21179, and 2MASS J08411840+1915394. Of these eight stars, five are from Hyades, two are from Praesepe, and one is from Coma Ber.

#### 3.2. Comparison of results from the three clusters

To first order, we have assumed that the data for all three clusters are homogeneous. This assumption can be tested by considering them individually. In addition to our overall  $\sigma = 0.031$  we also calculate  $\sigma$  for each individual cluster, applying a gaussian fit to the data in each cluster separately. We exclude stars that are  $> +3\sigma$  from the photospheric locus using the original  $\sigma$  value and obtain a new  $\sigma$  value for each cluster. Given the small number of sources in the individual clusters, the differences in the scatter around the main sequence locus (see Figure 3) are not very significant. Nonetheless, we tested if the individual values would change any of our results. For

Hyades we find  $\sigma = 0.027$ ; however, adopting this value does not allow us to identify any new excess sources. For Coma Ber we find  $\sigma = 0.036$ ; which is larger than the original value. However, the only source from Coma Ber with excess still remains beyond this new  $3\sigma$  threshold. Finally, for Praesepe we find  $\sigma = 0.032$ , which is similar to the overall average for the three clusters. We suspect that the differences in  $\sigma$  are due to small number statistics, but in any case they do not affect our conclusions.

### 3.3. Possible False Detections

A general possibility for false detections is confusion with background infrared-emitting galaxies. For this situation, we have adapted the analysis of Gáspár et al. (2009), adjusting for our smaller matching radius ( $1''.5$  vs.  $3''.6$ ). Because faint and distant galaxies are uniformly distributed over the sky, the analysis should apply to all three clusters. We find that there is a 10% probability of a single chance coincidence in our entire sample, and a 5% probability of two coincidences. We therefore make no corrections for such matches.

Plavchan et al. (2009) discuss the possibility that an M dwarf spectroscopic binary companion to a K dwarf may produce 10% “excess” (superphotospheric) flux at  $24\ \mu\text{m}$ . This would produce an artificial excess (false positive) source in our color-color space. There is only one known binary K star in our sample that shows an excess: HIP 21179 (Bender & Simon 2008). This star is considered to be a secure member of the Hyades (Perryman et al. 1998) with a relatively high X-ray luminosity (Stern et al. 1995). The masses of the components are  $0.79 \pm 0.08\ M_{\odot}$  and  $0.58 \pm 0.15\ M_{\odot}$  (Bender & Simon 2008). It is variable (V1147 Tau) with an amplitude in the visible of  $\sim 0.17$  mag (Watson et al. 2011). The HIP 21179 excess is  $6\sigma$  and 19% higher than the photospheric prediction, but given this list of issues we do not consider the presence of a debris disk to be secure and we discard it from our sample of disks.

The second late-type star with an apparent excess is HD 285690. It is also a secure Hyades member (Perryman et al. 1998), but has no evidence for binarity and is of low X-ray luminosity (Stern et al. 1995). Although it is variable (V985 Tau), the amplitude is only 0.02 mag (Watson et al. 2011), not at a level that significantly undermines the identification of the  $24\ \mu\text{m}$  excess. This star is therefore likely to be a genuine debris disk detection. The third such star, HD 286789, is also a secure Hyades member with low X-ray luminosity. It shows variability of 0.06 magnitudes in the visible (Watson et al. 2011), but given the general reduction in variability amplitude for late dwarf stars in the infrared (e.g., Koen et al. 2005), the excess is reasonably secure. Since the  $\chi^2$  value for the excess of HD 286789 is only slightly above 3, we combined the 2MASS H and K measurements (the error on J is large) to compute an equivalent K of  $7.792 \pm 0.022$ , and a new  $\chi^2$  of 3.7. Both of these stars are sufficiently bright at  $24\ \mu\text{m}$  that the probability of chance

coincidences with background galaxies that might create false excesses is small:  $\sim 1\%$  for one or more such coincidences in our entire sample (scaling from Gáspár et al. 2009). We therefore retain both stars in our sample.

### 3.4. Comparison to Previous Work

Our work is the first analysis of the *Spitzer* MIPS data for Coma Ber; however, the observations of the Hyades have been analyzed previously by Cieza et al. (2008) and Stauffer et al. (2010), while a paper on Praesepe has been published by Gáspár et al. (2009). In the Hyades, Cieza et al. (2008) found only a single star with a significant excess, HD 28355; this star is also found to have an excess by Su et al. (2006) and in our work. The identification of five additional stars with excesses by Stauffer et al. (2010) and by us results directly from the smaller RMS scatter in the data reduction and our more accurate extrapolation of the photospheric emission to  $24\ \mu\text{m}$ . Stauffer et al. (2010) found an excess for one case not in our sample, the F8V star, HD 26784. We agree that it has a nominal excess of  $\sim 0.09$  mag ( $K_S = 5.862$ ,  $[24] = 5.782$ , shift of  $-0.014$ ), near the threshold for detection, but it fell below our uniform threshold for an excess of  $0.1$  mag. The largest term in the uncertainty for this star is the 2MASS K magnitude. We have augmented it by using standard JHK colors (Tokunaga 2000, Carpenter et al. 2008, with the correction described in Rieke et al. 2008) appropriate for its V-K color ( $=1.26$ ) to compute equivalent K magnitudes from 2MASS J and H, assuming an additional uncertainty of  $0.01$  for J-K and  $0.005$  for H-K. A weighted average of the three measures yields  $K = 5.862 \pm 0.012$ , and confirms that an excess is detected for this star at a statistically significant level.

Gáspár et al. (2009) identified four stars with probable excesses in Praesepe; three of them (numbers 77, 134, and 181) do not pass the signal to noise threshold for inclusion in our sample. The remaining star, number 143 = 2MASSJ08411840+1915394, is also found to have an excess in our study, while our measurement of number 134 = 2MASS08410961+1951186 verifies its excess, even if its error in  $K_S - [24]$  was too large to include it in our sample. The remaining two sources, numbers 77 = 2MASS08395998+1934405 and 181 = 2MASS08424021+1907590, do not pass our criteria for firmly-established excesses because our noise estimation is significantly more conservative (larger noise) than that used by Gáspár et al. (2009).

### 3.5. Secondary sample

The case of HD 26784 suggests that there may be other plausible excesses below our overall threshold of  $K_S - [24] > 0.1$  and  $[24]$  error  $\leq 0.05$ . In fact, a search relaxing the requirements on



size of excess and  $K_S$  - [24] error yields Melotte 111 AV573 = 2MASS12133585+2910216 from Coma Ber as having evidence for a debris disk.

We divide the detected excesses into two samples. The primary one is defined by our initial criteria (excess at  $> 3 \sigma$  significance and  $> 0.1$  magnitudes), and can be compared directly with previous studies identifying excesses by similar criteria. The secondary sample consists of HD 26784 (F8V), Melotte 111 AV573 ( $\sim$  K0), and 2MASS08410961+1951186 ( $\sim$  G4 from its V-K color).

#### 4. Discussion

From our study, the overall rate of  $24\text{-}\mu\text{m}$  excesses  $> 10\%$  of the photospheric level at 670 Myr is  $5.7^{+3.1}_{-1.7}\%$  (7/122 sources). The errors (here and in the following) are calculated using a binomial distribution for small number statistics. Our result is higher than the excess rate for Praesepe of  $2.1^{+4.1}_{-2.1}\%$  (4/193 sources) found by Gáspár et al. (2009), but the difference can be largely explained by the smaller threshold for identifying an excess in our study (0.1 magnitudes instead of 0.15); in any case, the two values agree within the errors.

We now compare the evolution as a function of stellar type. A first-order estimate of the time scale for debris disk evolution is given by Wyatt (2008), equation (16). To apply this result, we assume an average luminosity ratio of 8 between our early-type (B9 - F4) and solar-like (F5 - K9) samples, and a mass ratio of 1.7. The thermal equilibrium distance from the fiducial stars is then different by a factor of 2.8. We assume that typical planetesimal disk masses scale with the mass of the star (Natta et al. 2000). We find that the time scale is dominated by the strong radial dependence in equation (16), which indicates that the decay around the early-type stars should be an order of magnitude slower than around the solar-like ones.

Our sample is ideally suited to determine the excess rate for stars near the mass of the sun and with well-constrained ages near 670 Myr. We used spectral types from SIMBAD and placed stars without a given spectral type from SIMBAD in bins according to their  $V - K_S$  colors using Table 3 in Koornneef (1983). We find that the excess rate for F5–K9 type stars is  $2.7^{+3.3}_{-1.7}\%$  (2/75 stars), in agreement with the value of  $1.9 \pm 1.2 \%$  from Gáspár et al. (2009). However, the secondary sample includes three well-detected debris disks around stars in the same spectral range, so this value may be a modest underestimate. We can compare it with that obtained by Sierchio et al. (2010), who measured the excess rate for stars in the same spectral range in the 115 Myr Pleiades cluster and the similar-age Blanco 1 association using the same reduction method and excess threshold of 10%. They report an excess rate of  $31.5^{+5.2}_{-4.5}\%$  at  $24 \mu\text{m}$  (28/89). We can add to their sample observations in the  $\alpha$  Per cluster (Carpenter et al. 2009) at an age of 85 Myr, for a total of  $29.4^{+4.9}_{-4.1}\%$  (30/102)

at an age of  $\sim 100$  Myr.

We have assembled similar data for B9–F4 stars from the literature. For the age range 50–99 Myr there are 17/47 stars with  $24 \mu\text{m}$  excesses, or  $36.2_{-6.2}^{+7.3}\%$  (Rieke et al. 2005; Su et al. 2006; Siegler et al. 2007; Balog et al. 2009), while in the 100–199 Myr range there are 33/93, or  $35.5_{-4.6}^{+5.1}\%$  (Rieke et al. 2005; Su et al. 2006; Gorlova et al. 2006). The combined result for 50–199 Myr is  $35.7_{-3.8}^{+4.3}\%$  (50/140). In the 400–1000 Myr range, the corresponding number is 6/77, or  $7.8_{-2.1}^{+4.2}\%$  (Su et al. 2006; this work). This value agrees well with that in Gáspár et al. (2009) of  $6.5 \pm 4.1 \%$ .

The incidence of debris disks at  $\sim 100$  Myr shows no difference between the two ranges of spectral type. At  $\sim 670$  Myr, the later spectral types show a lower incidence, but the two values still agree at the  $1.5 \sigma$  level. Moreover, the detection of three later-type stars in the secondary sample (of which HD 26784 only barely misses the primary sample) suggests that a significant number of such stars retain debris disks at this age. This conclusion has been reached previously (e.g., Trilling et al. (2008); Gáspár et al. (2009); Carpenter et al. (2009)).

However, all previous such works have depended in part or entirely on samples of field stars. Given the uncertainties in age estimates for these stars, combined with the rapid decline in the incidence of excesses (from  $\sim 30\%$  at 100 Myr to  $\sim 3 \%$  at 670 Myr), age errors that place a small number of young stars among the older part of a sample could yield the observed number of excesses. Our work removes this source of uncertainty by basing the result entirely on observations of cluster members with well-determined ages. Thus, the data appear to contradict the first-order theoretical time scale difference for disk decay as a function of stellar type.

## 5. Conclusion

We used  $24 \mu\text{m}$  *Spitzer* observations of stars in three clusters (Hyades, Coma Ber, and Praesepe) to measure the incidence of debris disks at  $\sim 670$  Myr and over a broad range of spectral types. The combination of three clusters at the same age gives a better representation of the excess behavior because we can use the closest cluster (Hyades) to detect excesses around low mass stars, while having access to significant numbers of higher mass stars in the more distant cluster (Praesepe). We compared the  $V-K_S$ ,  $K_S-[24]$  of the cluster members with the color locus of 1300 field stars. The dispersion around this locus is  $10\%$  ( $3\sigma$ ), which we adopt as the threshold for identification of an excess.

We find an overall excess rate of  $5.7_{-1.7}^{+3.1}\%$  for stars at  $\sim 670$  Myr. This value shows substantial decay from the rates of  $29.4_{-4.1}^{+4.9}\%$  for F5–K9 stars and  $35.7_{-3.8}^{+4.3}\%$  for B9–F4 stars at  $\sim 100$  Myr. However, the decay appears to be similar within the errors between these ranges of spectral types.

This result is contrary to first-order estimates, which would indicate an order-of-magnitude slower decay for the early type stars than the solar-like ones.

This work was supported at Northern Arizona University by funding from the Spitzer Science Center/JPL. Funding was also provided by the National Science Foundation through a Research Experience for Undergraduates (REU) position at Northern Arizona University. Support was also provided by contract 1255094 from Caltech/JPL to the University of Arizona. This research made use of the SIMBAD and Vizier database, operated at CDS, Strasbourg, France. This work also uses data products from the Two Micron All Sky Survey, which is a joint project of the University of Massachusetts and the Infrared Processing and Analysis Center/California Institute of Technology, funded by the National Aeronautics and Space Administration and the National Science Foundation. We would also like to thank Jennifer Sierchio and Andras Gáspár for helpful comments and discussions and the anonymous referee whose suggestions improved this paper.

## REFERENCES

- Abad, C., & Vicente, B. 1999, *VizieR Online Data Catalog*, 413, 60307
- Agnor, C. B., Canup, R. M., & Levison, H. F. 1999, *Icarus*, 142, 219
- Aumann, H. H., et al. 1984, *ApJ*, 278, L23
- Balog, Z., et al. 2009, *ApJ*, 698, 1989
- Bender, C. F., & Simon, M. 2008, *ApJ*, 689, 416
- Carpenter, J. M. et al. 2008, *ApJS*, 179, 423
- Carpenter, J. M., et al. 2009, *ApJS*, 181, 197
- Chambers, J. E. 2001, *Icarus*, 152, 205
- Cieza, L. A., Cochran, W. D., & Augereau, J.-C. 2008, *ApJ*, 679, 720
- Collier, C. A. et al. (2009), *MNRAS*, 400, 451
- Cutri, R. M. et al. (2003), *The IRSA 2MASS All-Sky Point Source Catalog*, NASA/IPAC
- Decin, G., Dominik, C., Malfait, K., Mayor, M., & Waelkens, C. 2000, *A&A*, 357, 533
- Decin, G., Dominik, C., Waters, L. B. F. M., & Waelkens, C. 2003, *ApJ*, 598, 636
- De Gennaro, S., von Hippel, T., Jeffreys, W. H., Stein, N., van Dyk, D., & Jeffrey, E. 2009, *ApJ*, 696, 12
- Dominik, C., & Decin, G. 2003, *ApJ*, 598, 626
- Engelbracht, C. M. et al. 2007, *PASP*, 119, 994
- Hahn, J. M., & Malhotra, R. 1999, *AJ*, 117, 3041
- Gáspár, A., Rieke, G. H., Su, K. Y. L., Balog, Z., Trilling, D., Muzzerole, J., Apai, D., & Kelly, B. C. 2009, *ApJ*, 697, 1578
- Gomes, R. S., Morbidelli, A., & Levison, H. F. 2004, *Icarus*, 170, 492
- Gorlova, N., Rieke, G. H., Muzerolle, J., Stauffer, J. R., Siegler, N., Young, E. T., & Stansberry, J. H. 2006, *ApJ*, 649, 1028
- Gordon, K. D. et al. 2005, *PASP*, 117, 503

- Habing, H. J., et al. 2001, *A&A*, 365, 545
- Haisch, K. E., Jr., Lada, E. A., & Lada, C. J. 2001, *ApJ*, 553, L153
- Kenyon, S. J., & Bromley, B. C. 2004, *ApJ*, 602, 133
- Koen, C., Tanabé, T., Tamura, M., & Kusakabe, N. 2005, *MNRAS*, 362, 727
- Koerner, D. W., et al. 2010, *ApJ*, 710, L26
- Koornneef, J. 1983, *A&AS*, 51, 489
- Lagrange, A.-M., Backman, D. E., & Artymowicz, P. 2000, *Protostars and Planets IV*, 639
- Levison, H. F., Morbidelli, A., Gomes, R., & Backman, D. 2007, *Protostars and Planets V*, 669
- Meyer, M. R., et al. 2008, *ApJ*, 673, L181
- Morales, F. Y., Rieke, G. H., Werner, M. W., Bryden, G., Stapelfeldt, K. R., & Su, K. Y. L. 2011, *ApJ*, 730, L29
- Morishima, R., Stadel, J., & Moore, B. 2010, *Icarus*, 207, 517
- Natta, A., Grinin, V., & Mannings, V. 2000, *Protostars & Planets IV* (Tucson: U. Ariz. Press), p. 559
- Paulson, D. B., Cochran, W. D., & Hatzes, A. P. 2004, *AJ*, 127, 3579
- Perryman, M. A. C., et al. 1997, *A&A*, 323, L49
- Perryman, M. A. C., et al. 1998, *A&A*, 331, 81
- Plavchan, P., Werner, M. W., Chen, C. H., Stapelfeldt, K. R., Su, K. Y. L., Stauffer, J. R., & Song, I. 2009, *ApJ*, 698, 1068
- Raymond, S. N., Quinn, T., & Lunine, J. I. 2006, *Icarus*, 183, 265
- Rhee, J. H., Song, I., Zuckerman, B., & McElwain, M. 2007, *ApJ*, 660, 1556
- Rieke, G. H., et al. 2004, *ApJS*, 154, 25
- Rieke, G. H., et al. 2005, *ApJ*, 620, 1010
- Rieke, G. H., et al. 2008, *AJ*, 135, 2245
- Siegler, N. et al. 2007, *ApJ*, 654, 580

- Sierchio, J. M., Rieke, G. H., Su, K. Y. L., Plavchan, P., Stauffer, J. R., & Gorlova, N. I. 2010, *ApJ*, 712, 1421
- Spangler, C., Sargent, A. I., Silverstone, M. D., Becklin, E. E., & Zuckerman, B. 2001, *ApJ*, 555, 932
- Stauffer, J. R., et al. 2010, *ApJ*, 719, 1859
- Stern, R. A., Schmitt, J. H. M. M., & Kahabka, P. T. 1995, *ApJ*, 448, 683
- Su, K. Y. L., et al. 2006, *ApJ*, 653, 675
- Su, K. Y. L. et al. (2010)] Su, K. Y. L. et al. 2010, AAS Meeting 215, abs. 428.26
- Taylor, B. J. 2006, *AJ*, 132, 2453
- Tokunaga, A. T. 2000, in *Allens Astrophysical Quantities*, 4th Ed. (New York: AIP Press), p 143.
- Trilling, D. E., et al. 2008, *ApJ*, 674, 1086
- Watson, C., Henden, A. A., & Price, A. 2011, AAVSO Variable Star Index (online at [VizieR](#))
- Wyatt, M. C. 2008, *ARA&A*, 46, 339

Table 1. Cluster Stars Considered

Name	Sp Type	V	$K_S$	$K_{err}$	f24	[24]	$[24]_{err}$	$(K-[24])_{err}$	Incl?	Excl. note	Cluster
Cl* Melotte 111 AV1119	G5V	10.830	9.295	0.019	1.453	9.233	0.057	0.060	n	4	c
Cl* Melotte 111 AV1183	K3V	11.500	8.972	0.020	1.932	8.924	0.043	0.047	y	...	c
Cl* Melotte 111 AV1280	K4V:	11.720	9.476	0.018	1.164	9.474	0.068	0.070	n	1,2,4	c
Cl* Melotte 111 AV1284	F2	4.780	3.236	0.244	395.500	3.146	0.011	0.244	n	4	c
Cl* Melotte 111 AV1288	G0	12.520	10.519	0.019	...	...	0.011	0.022	n	3	c
Cl* Melotte 111 AV1292	F8V	10.990	9.606	0.021	1.047	9.589	0.077	0.080	n	4	c
Cl* Melotte 111 AV1293	G5V:	12.580	10.796	0.024	0.359	10.750	0.132	0.135	n	4	c
Cl* Melotte 111 AV1297	G8V	10.440	8.752	0.021	2.418	8.680	0.070	0.073	n	4	c
Cl* Melotte 111 AV1420	K2V:	11.220	9.078	0.020	1.768	9.020	0.044	0.048	y	...	c
Cl* Melotte 111 AV1435	K2V:	11.490	9.424	0.018	1.214	9.428	0.066	0.068	n	1,4	c
Cl* Melotte 111 AV1464	...	11.430	9.417	0.025	1.190	9.450	0.148	0.150	n	2,4	c
Cl* Melotte 111 AV1487	K0V:	...	10.813	0.018	0.348	10.784	0.132	0.133	n	4,5	c
Cl* Melotte 111 AV1537	G5V:	11.300	9.844	0.024	0.814	9.862	0.094	0.097	n	4	c
Cl* Melotte 111 AV1548	G8V:	12.720	10.722	0.022	0.371	10.714	0.124	0.126	n	1,2,4	c
Cl* Melotte 111 AV1561	G5V:	11.560	10.023	0.024	0.712	10.008	0.112	0.115	n	4	c
Cl* Melotte 111 AV1584	G0V:	12.010	10.416	0.021	0.462	10.478	0.123	0.125	n	1,4	c
Cl* Melotte 111 AV1623	K2V:	12.530	10.270	0.021	0.586	10.219	0.131	0.132	n	1,4	c
Cl* Melotte 111 AV1695	G0V:	11.790	10.315	0.021	0.647	10.111	0.120	0.121	n	4	c
Cl* Melotte 111 AV1711	G8V:	11.880	9.970	0.021	0.811	9.867	0.094	0.096	n	4	c
Cl* Melotte 111 AV1768	G5V:	12.130	10.568	0.021	0.427	10.563	0.111	0.113	n	4	c
Cl* Melotte 111 AV190	...	...	9.224	0.018	1.453	9.233	0.122	0.123	n	4,5	c
Cl* Melotte 111 AV1966	G5V:	12.520	10.848	0.023	0.462	10.478	0.111	0.113	n	1,4	c
Cl* Melotte 111 AV2049	G8V:	12.200	10.637	0.021	0.500	10.391	0.101	0.103	n	1,2,4	c
Cl* Melotte 111 AV2062	K0V:	11.320	8.995	0.019	1.823	8.987	0.045	0.049	y	...	c
Cl* Melotte 111 AV2331	G7V	11.890	10.205	0.021	0.618	10.161	0.130	0.132	n	2,4	c
Cl* Melotte 111 AV472	...	12.840	10.895	0.017	0.331	10.839	0.153	0.154	n	4	c
Cl* Melotte 111 AV477	G5V:	12.070	10.518	0.017	0.444	10.521	0.114	0.115	n	4	c
Cl* Melotte 111 AV481	G0V:	12.230	10.511	0.016	0.489	10.416	0.112	0.113	n	1,2,4	c
Cl* Melotte 111 AV484	F5	11.970	10.826	0.017	0.269	11.065	0.189	0.190	n	1,2,4	c
Cl* Melotte 111 AV497	G0V:	12.430	10.840	0.019	0.312	10.903	0.161	0.163	n	4	c
Cl* Melotte 111 AV501	G8V:	12.660	10.766	0.019	0.399	10.636	0.122	0.124	n	2,4	c
Cl* Melotte 111 AV519	G5V:	11.910	9.630	0.016	1.212	9.430	0.067	0.069	n	4	c
Cl* Melotte 111 AV551	G0V:	11.850	10.531	0.018	0.483	10.430	0.109	0.110	n	1,2,4	c
Cl* Melotte 111 AV569	G0V:	12.510	10.741	0.019	0.410	10.606	0.115	0.117	n	4	c
Cl* Melotte 111 AV571	G0V:	12.630	10.424	0.018	0.419	10.583	0.143	0.144	n	2,4	c
Cl* Melotte 111 AV573	K0V:	11.480	9.415	0.018	1.496	9.201	0.054	0.057	n	4	c
Cl* Melotte 111 AV605	G0V:	11.090	9.717	0.017	0.895	9.760	0.092	0.094	n	4	c
Cl* Melotte 111 AV610	K4V:	10.940	7.542	0.020	7.923	7.392	0.024	0.031	y	...	c
Cl* Melotte 111 AV669	G0V:	11.420	9.813	0.016	0.832	9.838	0.097	0.099	n	4	c
Cl* Melotte 111 AV726	G0V:	11.220	9.671	0.018	0.926	9.722	0.092	0.093	n	1,2,4	c
Cl* Melotte 111 AV773	K0V:	11.200	9.332	0.020	1.261	9.387	0.062	0.065	n	1,2,4	c
Cl* Melotte 111 AV838	G5V:	11.940	10.328	0.018	0.477	10.443	0.126	0.127	n	2,4	c
Cl* Melotte 111 AV967	...	...	11.646	0.021	0.270	11.059	0.206	0.207	n	2,4,5	c
BD+25 2478	A0V	10.640	10.629	0.014	0.593	10.207	0.087	0.088	n	1,2,4	c
BD+25 2485	G7V	9.400	7.165	0.020	9.724	7.169	0.020	0.029	y	...	c

Table 1—Continued

Name	Sp Type	V	$K_S$	$K_{err}$	$f_{24}$	[24]	$[24]_{err}$	$(K-[24])_{err}$	Incl?	Excl. note	Cluster
BD+25 2509	G8V	11.340	9.208	0.019	1.557	9.158	0.054	0.057	n	4	c
BD+26 2303	F8V	10.050	8.802	0.017	2.134	8.816	0.082	0.083	n	4	c
BD+26 2310	G5V	10.980	9.389	0.018	1.231	9.413	0.070	0.072	n	4	c
BD+26 2312	K1V	9.560	6.104	0.016	28.860	5.988	0.012	0.020	y	...	c
BD+26 2333	F8V	10.360	8.793	0.024	2.086	8.841	0.081	0.084	n	4	c
BD+26 2336	F3V	9.570	8.456	0.019	2.984	8.452	0.062	0.065	n	1,4	c
BD+26 2339	F5V	10.040	8.903	0.022	1.730	9.044	0.102	0.105	n	2,4	c
BD+26 2342	K0V	10.470	8.611	0.021	2.248	8.759	0.077	0.080	n	2,4	c
BD+28 2091	F8V	10.020	8.750	0.021	2.230	8.768	0.079	0.081	n	1,4	c
GJ9410	K4V	11.090	8.146	0.023	4.264	8.064	0.039	0.045	y	...	c
GSC01988-00346	G5V:	11.940	10.171	0.018	0.679	10.059	0.115	0.116	n	2,4	c
GSC01991-00357	G5V:	11.850	10.339	0.018	0.277	11.032	0.201	0.201	n	1,2,4	c
GSC01991-00612	G5V:	12.660	10.796	0.018	0.336	10.823	0.137	0.138	n	1,2,4	c
GSC01991-00727	G0V:	11.560	10.068	0.028	0.735	9.973	0.108	0.111	n	4	c
HD105371	F6V	8.500	7.292	0.024	8.128	7.364	0.024	0.034	y	...	c
HD105805	A4Vn	6.010	5.600	0.033	38.720	5.669	0.012	0.035	y	...	c
HD105898	G2V	7.510	5.307	0.017	55.610	5.276	0.011	0.020	y	...	c
HD106293	F5V	8.080	6.990	0.033	11.320	7.004	0.019	0.038	y	...	c
HD106691	F5IV	8.090	7.036	0.017	10.550	7.081	0.020	0.026	y	...	c
HD106857	F5V	8.960	7.726	0.018	5.988	7.696	0.030	0.035	n	1	c
HD106946	F2V	7.850	6.928	0.017	12.110	6.931	0.018	0.025	y	...	c
HD106947	F7V	8.690	7.371	0.021	7.466	7.456	0.026	0.033	y	...	c
HD107086	F8V	7.560	6.474	0.031	17.760	6.515	0.014	0.034	y	...	c
HD107159	A5V	7.770	7.006	0.029	11.410	6.996	0.019	0.035	y	...	c
HD107214	G0V	9.020	7.492	0.027	7.086	7.513	0.027	0.038	y	...	c
HD107427	A3V	9.060	8.746	0.018	2.150	8.808	0.080	0.082	n	1,2,4	c
HD107611	F6V	8.510	7.325	0.020	8.409	7.327	0.022	0.030	n	1	c
HD107655	A0V	6.210	6.167	0.024	22.640	6.252	0.013	0.027	y	...	c
HD107701	F7V	8.550	7.024	0.018	11.210	7.015	0.020	0.027	y	...	c
HD107793	F8V	9.100	7.685	0.023	6.434	7.618	0.029	0.037	n	1	c
HD108007	A7V+...	6.410	5.731	0.016	33.560	5.824	0.012	0.020	n	2	c
HD108382	A4V	4.980	4.649	0.024	118.800	4.452	0.011	0.026	y	...	c
HD108945	A2pv	5.470	5.269	0.017	55.360	5.281	0.011	0.020	n	1	c
HD108956	F8V	7.120	5.609	0.026	41.730	5.588	0.012	0.028	y	...	c
HD108976	F6V	8.560	7.404	0.018	7.845	7.402	0.024	0.030	y	...	c
HD109127	F3V	9.070	8.236	0.017	3.540	8.266	0.051	0.054	n	2,4	c
HD109306	F3V	8.610	7.702	0.016	6.165	7.664	0.029	0.033	y	...	c
HD109307	A4Vm	6.280	5.989	0.026	27.130	6.055	0.013	0.029	y	...	c
HD116706	A3IV	5.750	5.502	0.018	42.310	5.573	0.012	0.021	y	...	c
HD018632	G5	7.970	5.841	0.024	34.390	5.798	0.012	0.027	y	...	h
HD020430	F8V	7.380	5.992	0.021	28.180	6.014	0.012	0.024	n	2	h
HD025825	G0	7.850	6.446	0.024	18.890	6.448	0.015	0.029	y	...	h
HD026767	G0	8.050	6.534	0.017	17.570	6.527	0.016	0.023	y	...	h
HD026784	F8V	7.110	5.862	0.017	34.900	5.782	0.012	0.021	y	...	h
HD027250	G5	8.620	6.921	0.016	12.320	6.912	0.021	0.026	n	1	h



Table 1—Continued

Name	Sp Type	V	$K_S$	$K_{err}$	$f_{24}$	[24]	$[24]_{err}$	$(K-[24])_{err}$	Incl?	Excl. note	Cluster
HD027282	G8V	8.470	6.787	0.016	13.800	6.789	0.019	0.024	y	...	h
HD027406	G0V	7.460	6.124	0.018	26.200	6.093	0.014	0.023	y	...	h
HD027628	A3m	5.720	4.960	0.017	73.770	4.969	0.011	0.020	y	...	h
HD027685	G4V	7.860	6.203	0.018	23.970	6.190	0.012	0.022	y	...	h
HD027732	G5	8.840	7.121	0.016	10.350	7.101	0.023	0.028	y	...	h
HD027749	A1m	5.640	4.945	0.021	72.680	4.985	0.011	0.024	y	...	h
HD027771	G5	9.110	7.145	0.017	9.956	7.144	0.024	0.030	y	...	h
HD027808	F8V	7.130	5.871	0.020	31.180	5.904	0.013	0.024	y	...	h
HD027835	G2V	8.203	6.797	0.026	13.520	6.811	0.015	0.030	y	...	h
HD027859	G2V	7.790	6.290	0.016	22.450	6.261	0.013	0.020	y	...	h
HD027962	A2IV	4.300	4.098	0.029	151.700	4.186	0.011	0.031	y	...	h
HD027990	K2V	8.990	6.767	0.021	14.200	6.758	0.015	0.026	y	...	h
HD028068	G1V	8.040	6.436	0.027	20.060	6.383	0.013	0.030	y	...	h
HD028099	G2V	8.100	6.547	0.021	16.660	6.585	0.014	0.025	y	...	h
HD028205	G0	7.410	6.141	0.024	24.500	6.166	0.014	0.028	y	...	h
HD028226	Am	5.720	5.055	0.018	74.370	4.960	0.011	0.021	y	...	h
HD028237	F8	7.490	6.158	0.017	24.230	6.178	0.012	0.021	n	1	h
HD028258	G5	9.020	7.003	0.021	12.060	6.935	0.020	0.029	y	...	h
HD028344	G2V	7.830	6.404	0.020	20.130	6.379	0.013	0.024	y	...	h
HD028355	A7V	5.020	4.534	0.033	138.300	4.287	0.011	0.035	y	...	h
HD028462	K1V	9.080	7.139	0.024	10.290	7.108	0.017	0.030	y	...	h
HD028527	A6IV	4.780	4.364	0.036	122.800	4.416	0.011	0.038	y	...	h
HD028546	Am	5.470	4.903	0.023	75.950	4.937	0.011	0.026	y	...	h
HD028593	G5	8.590	6.884	0.023	12.530	6.894	0.020	0.030	y	...	h
HD028635	F8	7.780	6.455	0.021	18.640	6.463	0.013	0.025	y	...	h
HD028783	K0	8.929	6.770	0.016	14.860	6.709	0.014	0.022	n	2	h
HD028805	G5	8.641	6.941	0.026	11.920	6.948	0.016	0.031	y	...	h
HD028878	G5	9.357	7.351	0.024	8.431	7.324	0.020	0.031	y	...	h
HD028977	K0	9.644	7.553	0.026	7.076	7.514	0.024	0.035	y	...	h
HD028992	F8	7.900	6.445	0.026	18.940	6.445	0.014	0.029	y	...	h
HD029159	K0	9.345	7.373	0.015	8.087	7.369	0.021	0.026	y	...	h
HD029388	A6V	4.270	4.105	0.334	187.200	3.958	0.011	0.334	n	4	h
HD029461	G5	7.960	6.443	0.021	19.370	6.421	0.013	0.025	y	...	h
HD029488	A5Vn	4.670	4.229	0.036	145.400	4.232	0.011	0.038	y	...	h
HD030210	Am	5.350	4.974	0.020	70.940	5.012	0.011	0.023	y	...	h
HD030246	G5	8.300	6.738	0.033	14.070	6.768	0.015	0.036	y	...	h
HD030505	F5	8.980	7.059	0.026	11.000	7.035	0.017	0.031	y	...	h
HD030589	F8	7.720	6.355	0.016	19.960	6.388	0.015	0.022	y	...	h
HD030809	F8	7.900	6.671	0.021	15.820	6.641	0.017	0.027	y	...	h
HD031609	G5	8.890	7.235	0.017	9.617	7.181	0.023	0.029	y	...	h
HD032347	K0	9.000	7.226	0.027	9.029	7.250	0.024	0.036	n	2	h
HD033254	A2m	5.430	4.861	0.023	77.810	4.911	0.011	0.026	y	...	h
HD240648	K0	8.820	7.128	0.017	9.941	7.145	0.023	0.028	y	...	h
HD242780	K0	9.030	7.302	0.021	8.794	7.278	0.027	0.034	n	2	h
HD283704	G5	9.190	7.462	0.029	7.711	7.421	0.029	0.041	y	...	h

Table 1—Continued

Name	Sp Type	V	$K_S$	$K_{err}$	f24	[24]	$[24]_{err}$	$(K-[24])_{err}$	Incl?	Excl. note	Cluster
HD284552	K0	10.690	7.686	0.026	6.528	7.602	0.033	0.042	n	1	h
HD284653	K2V	10.690	7.995	0.033	4.578	7.987	0.034	0.047	y	...	h
HD284930	K0	10.290	7.742	0.020	5.629	7.763	0.028	0.034	n	2	h
HD285252	K2	8.990	6.910	0.021	11.980	6.943	0.020	0.029	y	...	h
HD285367	K2	9.310	7.254	0.023	9.446	7.201	0.019	0.030	y	...	h
HD285690	K0	9.570	7.322	0.017	9.825	7.158	0.024	0.029	y	...	h
HD285773	G5	8.950	7.055	0.027	10.890	7.046	0.017	0.032	y	...	h
HD285830	K0	9.480	7.348	0.020	8.338	7.336	0.026	0.033	y	...	h
HD285876	K0	11.020	7.895	0.024	5.171	7.855	0.032	0.040	n	1	h
HD285931	K1	8.480	6.465	0.024	18.660	6.462	0.013	0.027	y	...	h
HD286363	M0	10.120	7.574	0.021	6.906	7.541	0.022	0.031	y	...	h
HD286554	M0V	11.280	8.046	0.027	4.939	7.905	0.045	0.052	n	...	h
HD286734	K5.5	10.890	7.786	0.021	6.130	7.670	0.036	0.042	y	...	h
HD286789	K7	10.480	7.795	0.031	6.312	7.638	0.026	0.040	y	...	h
HD286929	K5	10.040	7.480	0.023	7.508	7.450	0.029	0.037	n	1,2	h
HIP13600	K0	8.830	7.179	0.024	9.780	7.163	0.023	0.033	y	...	h
HIP13806	G5	8.920	6.905	0.023	12.350	6.910	0.018	0.029	y	...	h
HIP15563	M0	9.650	6.881	0.023	13.320	6.828	0.018	0.029	y	...	h
HIP16529	G5	8.880	6.907	0.016	12.230	6.920	0.019	0.025	y	...	h
HIP17766	M1V	10.850	7.509	0.016	7.734	7.418	0.026	0.030	n	2	h
HIP18018	K7	10.170	7.395	0.020	8.108	7.367	0.027	0.033	n	2	h
HIP18946	K5	10.120	7.600	0.020	6.963	7.532	0.024	0.031	n	2	h
HIP19082	...	11.410	8.107	0.026	4.473	8.012	0.036	0.044	n	1	h
HIP19441	K5V	10.100	7.264	0.020	9.812	7.159	0.023	0.031	n	2	h
HIP21179	K0	11.000	7.654	0.020	8.313	7.339	0.014	0.024	y	...	h
HIP22177	K4.5	10.920	7.826	0.020	5.617	7.765	0.025	0.032	y	...	h
HIP23312	K2	9.710	7.589	0.026	6.553	7.598	0.022	0.034	y	...	h
2MASSJ08362985+1857570	F6V	9.409	8.300	0.021	3.599	8.248	0.070	0.073	n	4	p
2MASSJ08364896+1915265	G4V	11.180	9.690	0.022	...	...	...	...	n	2,4,6	p
2MASSJ08370203+1936171	F6V	9.182	8.060	0.020	4.249	8.068	0.056	0.059	n	4	p
2MASSJ08371635+1929103	K6V	99.990	10.470	0.019	0.547	10.293	0.306	0.306	n	2,4	p
2MASSJ08371829+1941564	G5V	11.440	9.800	0.019	0.937	9.709	0.182	0.183	n	2,4	p
2MASSJ08372638+1929128	K5V	...	10.830	0.019	...	...	...	...	n	2,4,5,6	p
2MASSJ08372755+1937033	G8V	11.650	9.810	0.018	0.846	9.820	0.183	0.184	n	2,4	p
2MASSJ08372793+1933451	F6V	9.790	8.460	0.020	2.754	8.539	0.052	0.056	n	4	p
2MASSJ08372819+1909443	F6V	9.500	8.400	0.021	3.043	8.430	0.050	0.055	n	4	p
2MASSJ08373381+2000492	F0Vn	8.698	7.950	0.033	4.770	7.942	0.046	0.057	n	4	p
2MASSJ08373624+1915542	...	13.470	10.760	0.022	...	...	...	...	n	3,4	p
2MASSJ08373699+1943585	Am	7.771	7.290	0.020	8.247	7.348	0.024	0.031	y	...	p
2MASSJ08374070+1931063	F0Vn	8.240	7.660	0.018	6.060	7.683	0.030	0.035	y	...	p
2MASSJ08374235+1908015	F4V	9.870	8.580	0.020	2.603	8.600	0.054	0.057	n	4	p
2MASSJ08374640+1935575	...	12.330	10.240	0.018	...	...	...	...	n	2,4	p
2MASSJ08374660+1926181	G0	10.660	9.280	0.024	1.352	9.311	0.113	0.115	n	4	p
2MASSJ08374675+1916020	A5V	6.720	6.170	0.018	24.711	6.157	0.017	0.024	y	...	p
2MASSJ08374739+1906247	...	12.280	10.200	0.018	...	...	...	...	n	2,4,6	p

Table 1—Continued

Name	Sp Type	V	$K_S$	$K_{err}$	$f_{24}$	[24]	$[24]_{err}$	$(K-[24])_{err}$	Incl?	Excl. note	Cluster
2MASSJ08374998+1953287	G	11.410	9.330	0.020	1.555	9.160	0.108	0.110	n	2,4	p
2MASSJ08375208+1959138	G5V	11.260	9.690	0.020	1.018	9.619	0.146	0.148	n	2,4	p
2MASSJ08375703+1914103	G8V	11.810	10.040	0.020	0.720	9.996	0.209	0.210	n	4	p
2MASSJ08380758+1959163	...	12.110	9.900	0.020	0.758	9.939	0.199	0.200	n	4	p
2MASSJ08380808+2026223	...	11.720	9.930	0.019	...	...	...	...	n	3,4,6	p
2MASSJ08381421+1947234	...	...	10.910	0.036	...	...	...	...	n	2,4,5,6	p
2MASSJ08381427+1921552	G5V	10.900	9.190	0.020	1.578	9.143	0.094	0.096	n	4	p
2MASSJ08382311+2012263	...	7.830	6.650	0.016	15.473	6.665	0.019	0.024	y	...	p
2MASSJ08382429+2006217	GOV	10.550	9.180	0.018	1.493	9.204	0.106	0.108	n	4	p
2MASSJ08382963+1951450	...	14.010	10.930	0.019	...	...	...	...	n	3,4	p
2MASSJ08383216+1927548	...	10.010	7.540	0.016	7.341	7.474	0.026	0.030	y	...	p
2MASSJ08383425+1951369	K0III	9.160	6.690	0.018	14.931	6.704	0.019	0.026	n	7	p
2MASSJ08383723+1901161	K5V	...	10.610	0.016	...	...	...	...	n	2,4,5,6	p
2MASSJ08383776+1938480	F6V	10.560	9.220	0.020	1.452	9.234	0.106	0.107	n	2,4	p
2MASSJ08383786+1959231	F0V	8.150	7.610	0.018	6.160	7.665	0.029	0.034	y	...	p
2MASSJ08384695+1930033	F4V	9.000	8.220	0.020	4.013	8.130	0.041	0.045	y	...	p
2MASSJ08385001+2004035	G0	10.800	9.370	0.018	1.237	9.408	0.117	0.118	n	2,4	p
2MASSJ08385354+1934170	K6V	14.070	10.960	0.022	...	...	...	...	n	3,4,6	p
2MASSJ08385506+1911539	K3V	10.140	8.040	0.018	4.873	7.919	0.035	0.040	y	...	p
2MASSJ08390185+2000194	K5V	11.880	9.070	0.018	1.788	9.008	0.084	0.086	n	2,4	p
2MASSJ08390228+1919343	K	12.390	10.260	0.019	0.632	10.137	0.247	0.247	n	3,4	p
2MASSJ08390283+1943289	F7V	9.299	8.120	0.021	4.287	8.058	0.040	0.045	y	...	p
2MASSJ08390321+2002376	...	14.410	11.050	0.020	...	...	...	...	n	3,4,6	p
2MASSJ08390359+1959591	A9V	8.315	7.770	0.018	5.758	7.738	0.030	0.035	y	...	p
2MASSJ08390411+1931216	K5V	13.750	10.860	0.016	...	...	...	...	n	3	p
2MASSJ08390523+2007018	F5V	9.383	8.410	0.027	3.101	8.410	0.050	0.056	n	4	p
2MASSJ08390612+1940364	A9Vn	7.446	6.710	0.018	14.274	6.752	0.018	0.026	y	...	p
2MASSJ08390649+1900360	...	...	11.300	0.022	...	...	...	...	n	3,4,5,6	p
2MASSJ08390909+1935327	A9V	8.500	7.880	0.026	4.964	7.899	0.036	0.045	y	...	p
2MASSJ08391014+1940423	F6	9.408	8.410	0.016	2.914	8.477	0.053	0.056	n	4	p
2MASSJ08391217+1906561	...	10.580	9.260	0.018	1.497	9.201	0.106	0.108	n	4	p
2MASSJ08391499+2012388	G5V	11.310	9.650	0.020	0.955	9.689	0.193	0.194	n	2,4	p
2MASSJ08391972+2003107	K0V	9.220	7.080	0.021	10.649	7.071	0.021	0.029	y	...	p
2MASSJ08392185+1951402	...	12.530	10.370	0.020	0.597	10.200	0.267	0.268	n	2,4	p
2MASSJ08392498+1927336	F7V	10.470	9.000	0.018	1.967	8.904	0.073	0.075	n	4	p
2MASSJ08392858+1928251	K	11.630	9.530	0.021	1.186	9.454	0.123	0.125	n	4	p
2MASSJ08392940+1947118	...	12.640	10.060	0.018	0.655	10.098	0.328	0.329	n	3,4	p
2MASSJ08393042+2004087	F8V	10.320	8.810	0.018	2.163	8.801	0.068	0.071	n	4	p
2MASSJ08393342+2010102	K2V	9.064	6.130	0.021	27.606	6.036	0.017	0.027	y	...	p
2MASSJ08393643+1915378	K7V	14.380	11.010	0.018	...	...	...	...	n	3,4	p
2MASSJ08393836+1926272	K3	12.630	10.290	0.020	...	...	...	...	n	3,4,6	p
2MASSJ08394265+1946425	F0III	6.650	6.000	0.018	28.102	6.017	0.016	0.024	n	7	p
2MASSJ08394279+2005103	A5V	7.728	7.160	0.020	9.327	7.214	0.022	0.030	y	...	p
2MASSJ08394333+1925121	K5V	11.410	7.900	0.023	...	...	...	...	n	4,6	p
2MASSJ08394466+1916308	A7Vn	7.676	7.090	9.998	9.436	7.202	0.022	9.998	n	4	p

Table 1—Continued

Name	Sp Type	V	$K_S$	$K_{err}$	f24	[24]	$[24]_{err}$	$(K-[24])_{err}$	Incl?	Excl. note	Cluster
2MASSJ08394575+1922011	G0	10.660	9.260	0.020	1.286	9.366	0.109	0.111	n	4	p
2MASSJ08395072+1932269	K0III	6.590	4.390	0.040	130.702	4.348	0.015	0.043	n	7	p
2MASSJ08395084+1933020	K	11.800	10.000	0.022	0.747	9.956	0.217	0.218	n	3,4	p
2MASSJ08395234+1918455	F5V	10.230	9.010	0.020	1.846	8.973	0.080	0.083	n	4	p
2MASSJ08395506+2003541	F4V	10.114	8.960	0.019	1.968	8.904	0.080	0.083	n	2,4	p
2MASSJ08395649+1933107	Am	7.320	6.790	0.020	12.802	6.871	0.020	0.028	y	...	p
2MASSJ08395777+1932293	Am	7.544	7.010	0.023	10.816	7.054	0.021	0.031	y	...	p
2MASSJ08395807+1912058	F6V	9.488	8.480	0.018	3.166	8.388	0.050	0.053	n	4	p
2MASSJ08395838+2009298	F2V	8.894	8.100	0.017	4.077	8.113	0.043	0.047	y	...	p
2MASSJ08395908+2001532	F5V	9.233	8.210	0.021	3.659	8.230	0.040	0.045	y	...	p
2MASSJ08395915+1940083	F3V	9.780	8.780	0.020	2.240	8.763	0.067	0.070	n	4	p
2MASSJ08395957+1856357	A3	9.960	9.300	0.017	1.411	9.265	0.139	0.140	n	4	p
2MASSJ08395983+1934003	K	11.920	9.480	0.018	1.251	9.396	0.117	0.119	n	4	p
2MASSJ08395998+1934405	...	12.860	10.550	0.018	0.561	10.267	0.250	0.251	n	3,4	p
2MASSJ08400062+1948235	F6V	10.300	9.080	0.020	1.776	9.015	0.091	0.094	n	4	p
2MASSJ08400130+2008082	F6V	9.670	8.620	0.018	2.665	8.575	0.058	0.061	n	4	p
2MASSJ08400171+1859595	F8V	10.020	8.700	0.018	2.704	8.559	0.072	0.074	n	4	p
2MASSJ08400416+1947039	...	12.060	10.000	0.020	0.642	10.120	0.225	0.226	n	4	p
2MASSJ08400491+1943452	F6V	9.790	8.650	0.020	2.572	8.613	0.060	0.063	n	4	p
2MASSJ08400571+1901307	...	12.640	10.010	0.020	0.749	9.952	0.209	0.210	n	2,4	p
2MASSJ08400627+1927148	F6V	10.240	8.870	0.020	2.048	8.861	0.075	0.077	n	4	p
2MASSJ08400635+1918264	G8V	11.010	9.230	0.018	1.454	9.232	0.108	0.110	n	4	p
2MASSJ08400643+2000280	G8III	6.390	4.200	0.027	154.238	4.168	0.015	0.031	n	77	p
2MASSJ08400968+1937170	...	11.980	10.130	0.020	0.556	10.277	0.294	0.295	n	3,4	p
2MASSJ08401145+1958161	A1V	6.610	6.530	0.023	16.269	6.610	0.019	0.030	y	...	p
2MASSJ08401231+1938222	F5V	9.903	8.670	0.023	2.483	8.651	0.063	0.067	n	4	p
2MASSJ08401345+1946436	...	13.190	10.640	0.020	...	...	...	...	n	3	p
2MASSJ08401535+1959394	F2V	8.809	8.040	9.995	4.185	8.085	0.040	9.995	n	4	p
2MASSJ08401549+1927310	K6V	13.920	10.690	0.020	...	...	...	...	n	3,4,6	p
2MASSJ08401571+1954542	...	12.700	10.010	0.018	0.713	10.005	0.205	0.206	n	2,4	p
2MASSJ08401762+1947152	F8V	9.960	8.580	0.018	2.486	8.650	0.063	0.066	n	4	p
2MASSJ08401810+1931552	F0III	7.540	7.160	0.017	9.251	7.223	0.022	0.028	n	7	p
2MASSJ08401893+2011307	K4V	12.970	10.040	0.018	0.958	9.685	0.156	0.157	n	3,4	p
2MASSJ08402013+1920564	A9V	6.760	6.040	0.017	27.407	6.044	0.016	0.024	y	...	p
2MASSJ08402075+1941120	F2III	7.680	7.280	0.023	8.416	7.326	0.023	0.032	n	7	p
2MASSJ08402209+1940116	G9III	6.420	4.180	0.036	163.650	4.104	0.015	0.039	n	7	p
2MASSJ08402231+2006243	F2III	10.057	8.850	0.018	2.249	8.759	0.064	0.067	n	1,4,7	p
2MASSJ08402271+1927531	...	10.700	9.340	0.020	1.482	9.212	0.101	0.102	n	2,4	p
2MASSJ08402327+1940236	F2	10.370	9.010	0.020	1.872	8.958	0.098	0.100	n	1,4	p
2MASSJ08402347+1950059	F2III	8.025	7.590	0.020	6.641	7.583	0.027	0.034	n	7	p
2MASSJ08402554+1928328	...	9.850	8.760	0.020	2.175	8.795	0.066	0.069	n	1,4	p
2MASSJ08402614+1941111	F6V	9.361	8.370	0.018	3.376	8.318	0.047	0.050	n	4	p
2MASSJ08402624+1913099	K3V	12.900	10.460	0.020	...	...	...	...	n	3,4,6	p
2MASSJ08402675+2010552	F2Vn	8.203	7.430	0.020	7.688	7.424	0.025	0.032	y	...	p
2MASSJ08402702+1932415	A5m	6.290	5.880	0.018	29.723	5.956	0.016	0.024	y	...	p

Table 1—Continued

Name	Sp Type	V	$K_S$	$K_{err}$	f24	[24]	$[24]_{err}$	$(K-[24])_{err}$	Incl?	Excl. note	Cluster
2MASSJ08402743+1916409	G5V	11.170	9.650	0.020	1.027	9.610	0.149	0.151	n	2,4	p
2MASSJ08402751+1939197	K4V	13.220	10.690	0.020	...	...	...	...	n	3	p
2MASSJ08402863+2018449	K	11.640	9.460	0.018	1.134	9.502	0.198	0.199	n	2,4	p
2MASSJ08403169+1951010	G9V	11.630	9.910	0.018	0.736	9.972	0.203	0.204	n	2,4	p
2MASSJ08403184+2012060	G5V	11.520	9.830	0.014	0.782	9.906	0.181	0.182	n	3,4	p
2MASSJ08403296+1911395	F0V	8.663	7.960	0.015	5.220	7.845	0.032	0.035	y	...	p
2MASSJ08403347+1938009	...	12.209	10.170	0.018	...	...	...	...	n	3	p
2MASSJ08403924+1913418	A9V	7.800	7.230	0.021	8.768	7.282	0.022	0.030	y	...	p
2MASSJ08403992+1940092	G3V	10.870	9.190	0.018	1.409	9.267	0.098	0.100	n	4	p
2MASSJ08404189+1913255	G1V	10.610	9.060	0.018	1.636	9.105	0.086	0.088	n	4	p
2MASSJ08404248+1933576	G6V	11.340	9.710	0.018	1.028	9.608	0.140	0.141	n	2,4	p
2MASSJ08404321+1943095	A9III	6.830	6.330	0.017	20.361	6.367	0.017	0.024	n	7	p
2MASSJ08404608+1918346	F6V	9.562	8.530	0.020	2.838	8.506	0.052	0.056	n	2,4	p
2MASSJ08404720+1932373	K3V	10.350	8.200	0.021	4.094	8.109	0.037	0.043	y	...	p
2MASSJ08404798+1939321	G7V	11.020	9.250	0.018	1.399	9.274	0.103	0.105	n	2,4	p
2MASSJ08404832+1955189	G3V	11.030	9.510	0.020	1.176	9.462	0.127	0.128	n	2,4	p
2MASSJ08405247+2015594	F0Vn	8.478	7.800	0.018	5.328	7.822	0.039	0.043	y	...	p
2MASSJ08405252+1928595	F7V	10.318	9.050	0.020	1.818	8.990	0.083	0.086	n	4	p
2MASSJ08405487+1956067	K1V	12.090	10.130	0.018	0.625	10.150	0.240	0.241	n	2,4	p
2MASSJ08405630+1934492	A6Vn	6.770	6.280	0.018	21.403	6.313	0.017	0.025	y	...	p
2MASSJ08405669+1944052	...	12.230	10.210	0.020	0.594	10.203	0.263	0.264	n	3,4	p
2MASSJ08405693+1956055	Am	8.713	8.050	0.023	4.497	8.006	0.034	0.041	y	...	p
2MASSJ08410478+1931225	G5V:	11.040	8.750	0.020	2.428	8.676	0.064	0.067	n	4	p
2MASSJ08410725+1926489	K1	12.430	10.290	0.018	0.631	10.139	0.328	0.329	n	3,4	p
2MASSJ08410737+1904164	G0	10.180	8.640	0.019	...	...	...	...	n	3	p
2MASSJ08410961+1951186	G	10.710	8.940	0.018	2.498	8.645	0.063	0.066	n	4	p
2MASSJ08410979+1956072	...	13.630	10.760	0.020	...	...	...	...	n	3,4,6	p
2MASSJ08411002+1930322	F6V	10.110	8.910	0.020	1.826	8.985	0.086	0.089	n	4	p
2MASSJ08411031+1949071	...	11.520	9.750	0.020	0.954	9.690	0.145	0.146	n	2,4	p
2MASSJ08411067+1949465	F5V	9.037	8.190	0.021	3.564	8.259	0.043	0.048	y	...	p
2MASSJ08411319+1932349	...	...	10.350	0.018	0.642	10.120	0.255	0.256	n	3,4,5	p
2MASSJ08411377+1955191	A5V	8.340	7.770	0.017	5.761	7.738	0.031	0.035	y	...	p
2MASSJ08411541+2002160	...	14.290	11.020	0.018	...	...	...	...	n	3,4,6	p
2MASSJ08411602+1944514	...	13.700	11.710	0.023	...	...	...	...	n	3,4,6	p
2MASSJ08411840+1915394	A7Vn	7.914	7.290	0.023	10.539	7.082	0.021	0.031	y	...	p
2MASSJ08411992+1938047	K5V	13.550	10.760	0.020	0.737	9.971	0.265	0.265	n	3,4	p
2MASSJ08412258+1856020	K3V	12.960	10.540	0.019	...	...	...	...	n	3,4,6	p
2MASSJ08412390+2014572	...	14.680	10.780	0.020	0.629	10.142	0.327	0.328	n	3,4	p
2MASSJ08412584+1956369	A2	10.720	9.330	0.020	1.172	9.467	0.128	0.130	n	4	p
2MASSJ08412698+1932329	F4V	9.880	8.720	0.020	2.081	8.843	0.071	0.074	n	4	p
2MASSJ08412869+1944481	G1V	10.930	9.470	0.018	1.085	9.551	0.148	0.150	n	4	p
2MASSJ08413384+1958087	...	11.710	9.930	0.018	0.734	9.975	0.205	0.206	n	3,4	p
2MASSJ08413506+1939449	K0III	8.500	5.960	0.023	31.178	5.904	0.016	0.028	n	7	p
2MASSJ08413599+1906255	...	14.170	10.980	0.018	...	...	...	...	n	3,4,6	p
2MASSJ08413620+1908335	F4V	9.320	8.350	0.022	3.126	8.401	0.048	0.053	n	4	p

Table 1—Continued

Name	Sp Type	V	$K_S$	$K_{err}$	f24	[24]	$[24]_{err}$	$(K-[24])_{err}$	Incl?	Excl. note	Cluster
2MASSJ08413741+1931140	K5V	13.570	10.730	0.018	0.522	10.345	0.296	0.297	n	3,4,6	p
2MASSJ08414229+1939379	F6V	9.590	8.480	0.019	...	...	...	...	n	4,6	p
2MASSJ08414368+1957437	...	12.360	10.260	0.019	0.599	10.194	0.373	0.374	n	3,4	p
2MASSJ08414382+2013368	F7	10.470	9.140	0.018	1.828	8.984	0.107	0.109	n	4	p
2MASSJ08414549+1916023	...	10.150	8.930	0.019	1.874	8.957	0.077	0.079	n	4	p
2MASSJ08414776+1924439	...	11.420	10.100	0.021	0.704	10.019	0.219	0.220	n	2,4	p
2MASSJ08414818+1927312	K5V	13.670	10.730	0.018	...	...	...	...	n	3	p
2MASSJ08414934+1911471	K8V	14.500	10.830	0.018	...	...	...	...	n	3,4,6	p
2MASSJ08415008+1952270	K0III	6.900	4.680	0.015	98.266	4.658	0.015	0.022	n	7	p
2MASSJ08415199+2010013	...	12.040	10.090	0.019	0.773	9.918	0.221	0.222	n	3,4,6	p
2MASSJ08415314+2009340	F2Vn	8.547	7.790	0.017	5.665	7.756	0.032	0.036	y	...	p
2MASSJ08415437+1915266	G5V	11.410	9.640	0.019	0.964	9.679	0.149	0.150	n	2,4	p
2MASSJ08415587+1941229	G5V	11.050	9.540	0.018	1.083	9.552	0.126	0.128	n	4	p
2MASSJ08415782+1854422	F5V	9.426	8.430	0.025	2.923	8.474	0.076	0.080	n	4	p
2MASSJ08415884+2006272	K4V	13.230	10.600	0.018	...	...	...	...	n	3,4,6	p
2MASSJ08420547+1935585	K0	10.630	8.380	0.031	3.414	8.306	0.050	0.058	n	4	p
2MASSJ08420650+1924405	A7V	7.954	7.430	0.024	7.589	7.438	0.024	0.034	y	...	p
2MASSJ08421080+1856037	A7Vn	7.900	7.350	0.020	7.986	7.383	0.031	0.037	y	...	p
2MASSJ08421149+1916373	...	12.150	10.170	0.016	...	...	...	...	n	4,6	p
2MASSJ08421233+1912488	K6V	13.700	10.830	0.016	...	...	...	...	n	3	p
2MASSJ08421285+1916040	K5V	13.500	10.480	0.014	0.663	10.086	0.213	0.213	n	2,4	p
2MASSJ08421549+1941156	...	9.880	8.770	0.016	2.173	8.796	0.065	0.067	n	4	p
2MASSJ08421883+2024350	...	12.420	10.190	0.019	...	...	...	...	n	3,4,6	p
2MASSJ08422012+2002117	F6V	9.724	8.410	0.021	3.100	8.411	0.048	0.052	n	4	p
2MASSJ08422162+2010539	F3Vn	9.226	8.280	0.021	3.836	8.179	0.043	0.048	y	...	p
2MASSJ08422471+1935175	...	10.990	9.480	0.014	1.337	9.323	0.113	0.114	n	4	p
2MASSJ08423225+1923463	...	10.990	9.460	0.016	1.224	9.419	0.125	0.126	n	4	p
2MASSJ08424021+1907590	...	12.150	10.190	0.018	0.652	10.103	0.227	0.227	n	3,4	p
2MASSJ08424071+1932354	F2III	9.770	8.720	0.018	2.453	8.665	0.063	0.066	n	2,4,7	p
2MASSJ08424250+1905589	...	11.620	9.880	0.021	0.880	9.777	0.170	0.171	n	4	p
2MASSJ08424372+1937234	...	12.120	9.800	0.020	1.092	9.543	0.132	0.134	n	2,4	p
2MASSJ08424441+1934479	F6V	9.740	8.630	0.018	2.818	8.514	0.054	0.056	n	4	p
2MASSJ08430055+2020161	G5V	11.440	9.770	0.020	1.017	9.621	0.222	0.223	n	2,4	p
2MASSJ08430593+1926152	F8V	9.970	8.460	0.021	3.105	8.409	0.051	0.055	n	4	p
2MASSJ08430822+1942475	K4V	13.330	10.670	0.017	...	...	...	...	n	3,4,6	p
2MASSJ08431076+1931346	...	11.780	10.010	0.021	0.595	10.203	0.239	0.240	n	3,4	p
2MASSJ08432019+1946086	...	10.770	9.360	0.018	1.392	9.280	0.111	0.112	n	4	p
2MASSJ08433239+1944378	K0V:	12.330	10.220	0.022	0.801	9.879	0.191	0.192	n	4	p
2MASSJ08433553+2011225	F6V	10.136	8.920	0.018	1.851	8.970	0.088	0.090	n	4	p
2MASSJ08440734+2004369	...	10.150	9.060	0.018	1.750	9.031	0.119	0.120	n	4	p

Note. — The characteristics of all stars in our sample. A total of 355 are presented here. Notes for column for reason for exclusion are as follows: (1) Contamination from nearby stars (2) FWHM much greater or much less than 5.5 arcsec (3) Signal to Noise < 3 (4) K-[24] error greater than .05 (5) No V mag (6) No 24  $\mu$ m counter part within 1''.5 search radius (7) Giant stars.

Table 2. Derived  $K_S - [24]$  shifts in each of the clusters

Cluster	Stars with $V - K_S \leq 0.8$	Stars with $V - K_S > 0.8$
Hyades	+0.011	−0.009
Coma Ber	+0.028	+0.011
Praesepe	+0.009	−0.014

Table 3. Identified 24  $\mu\text{m}$  excess sources

Name	Type	excess <sup>a</sup>	error <sup>b</sup>	$\chi_{24}$	Cluster	Previous ID
HD028226	Am	0.109	0.021	5.2	Hyades	Su et al. (2006)
HD028355	A7V	0.273	0.035	7.9	Hyades	Su et al. (2006)
HD285690	K0	0.155	0.029	5.3	Hyades	Stauffer et al. (2010)
HD286789	K7	0.127	0.040	3.7	Hyades	Stauffer et al. (2010)
HIP21179	K0	0.188	0.024	7.7	Hyades	none <sup>c</sup>
HD108382	A4V	0.252	0.026	9.5	Coma Ber	none
2MASSJ08385506+1911539	K3V	0.108	0.040	2.7	Praesepe	none <sup>d</sup>
2MASSJ08403296+1911395	F0V	0.125	0.035	3.6	Praesepe	none
2MASSJ08411840+1915394	A7V	0.223	0.031	7.2	Praesepe	Gáspár et al. (2009)
HD026784	F8V	0.094	0.017	5.5	Hyades	Stauffer et al. (2010) <sup>e</sup>
2MASS08410961+1951186	G	0.309	0.066	4.7	Praesepe	Gáspár et al. (2009) <sup>e</sup>
Melotte 111 AV573	$\sim$ K0	0.21	0.057	3.8	Coma Ber	none <sup>e</sup>

<sup>a</sup> $(K_S - [24])_{\text{observed}} - (K_S - [24])_{\text{predicted}}$ , in magnitudes

<sup>b</sup>Error calculated using Equation 1

<sup>c</sup>Excess probably not associated with a debris disk; see Section 3.3.

<sup>d</sup>Fails  $\chi_{24}$  test, see Section 3.1.

<sup>e</sup>Secondary sample; see Sections 3.4 & 3.5.

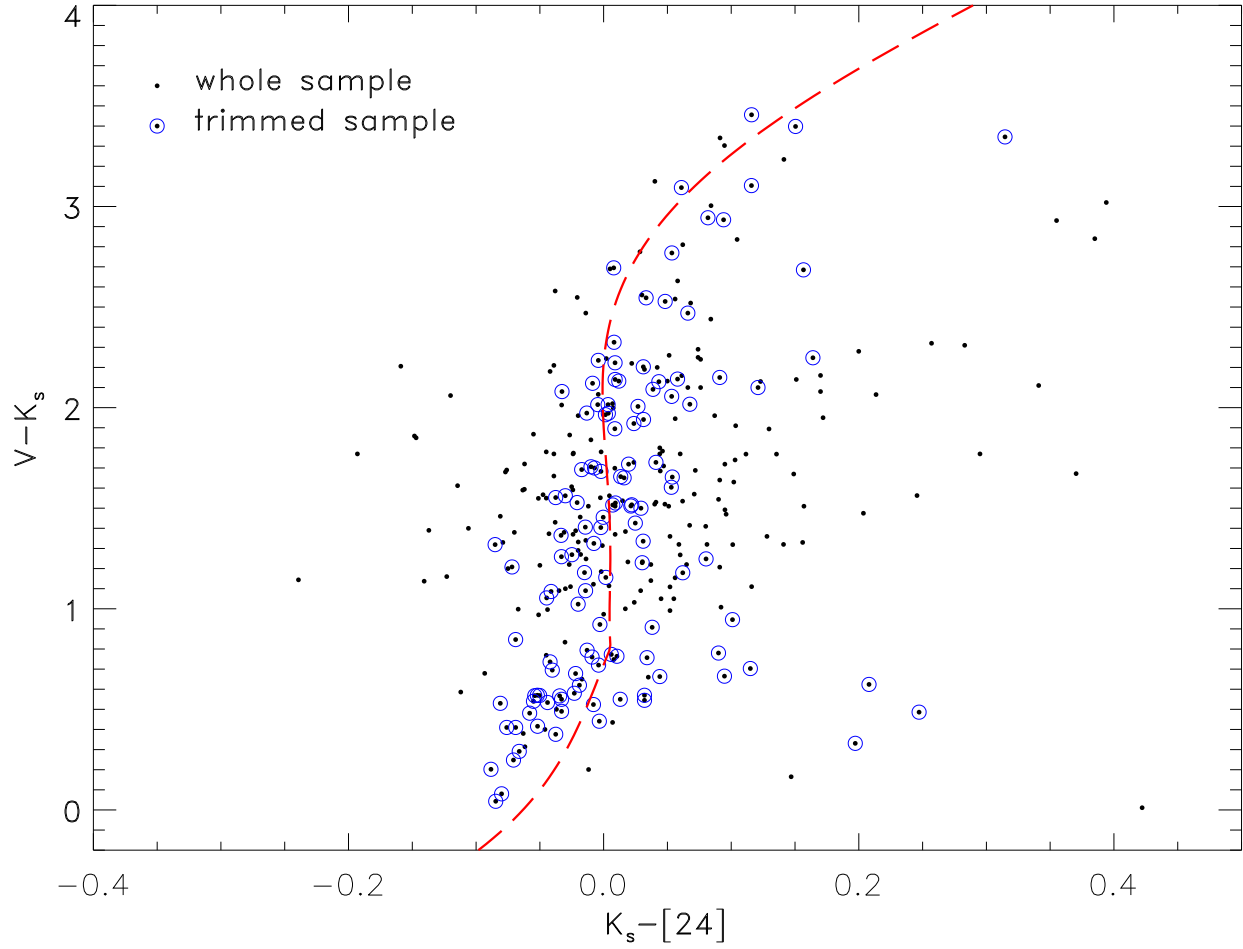


Fig. 1.—  $V - K_S$  vs.  $K_S - [24]$  color-color plot for 670 Myr cluster members. The entire sample is shown as small dots with circles indicating the ones retained in our analysis. The main-sequence locus presented in Eqn (2) and (3) is shown as the dashed line.



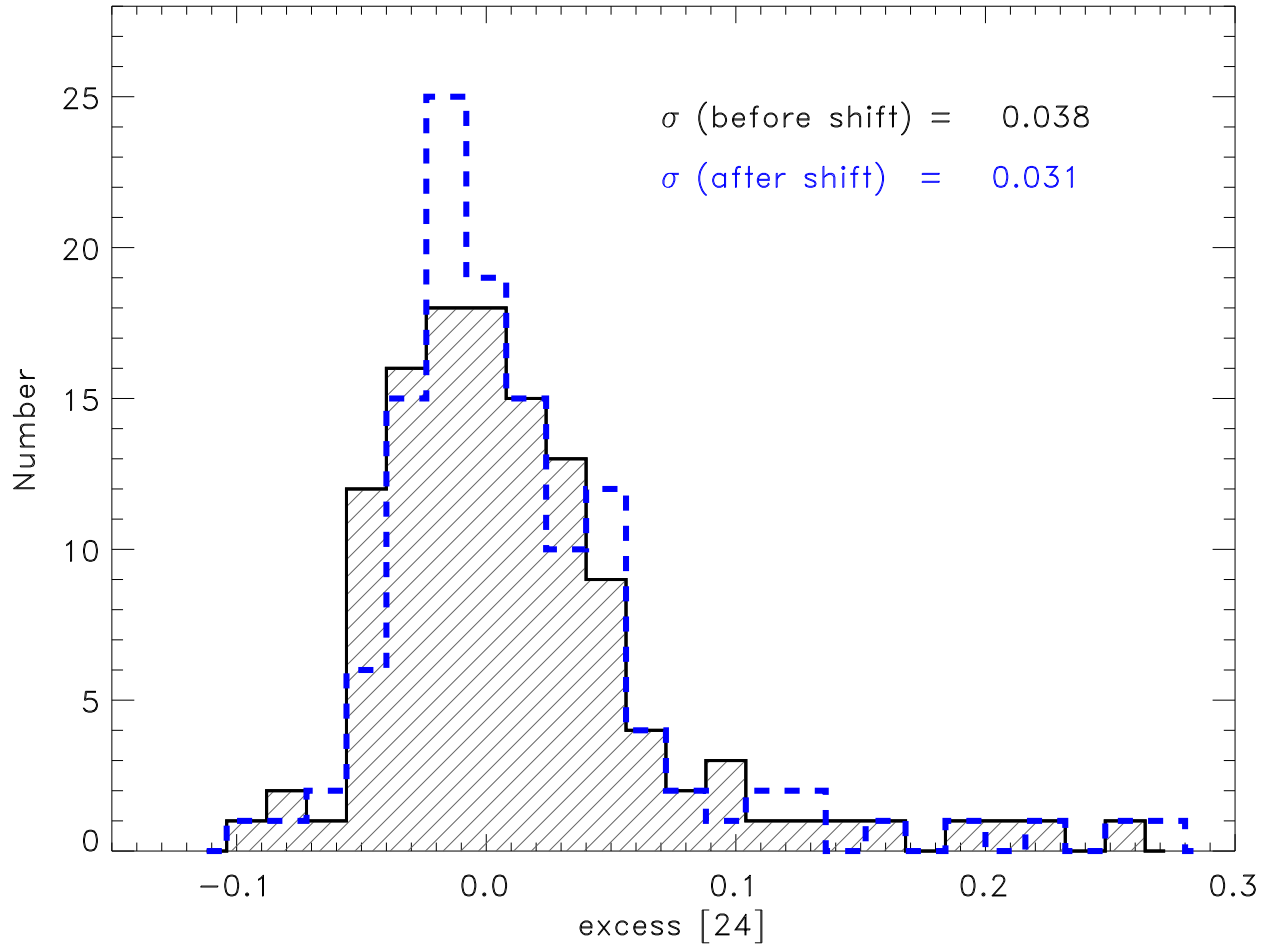


Fig. 2.— Histogram of  $V - [24]$  relative to the main sequence locus, for the stars retained in our analysis. The general nature of the distribution is similar before and after we shift the loci for the individual clusters to minimize the deviations from it. The stars with excesses are shown by the low-lying distribution extending to positive values  $> 0.1$ .

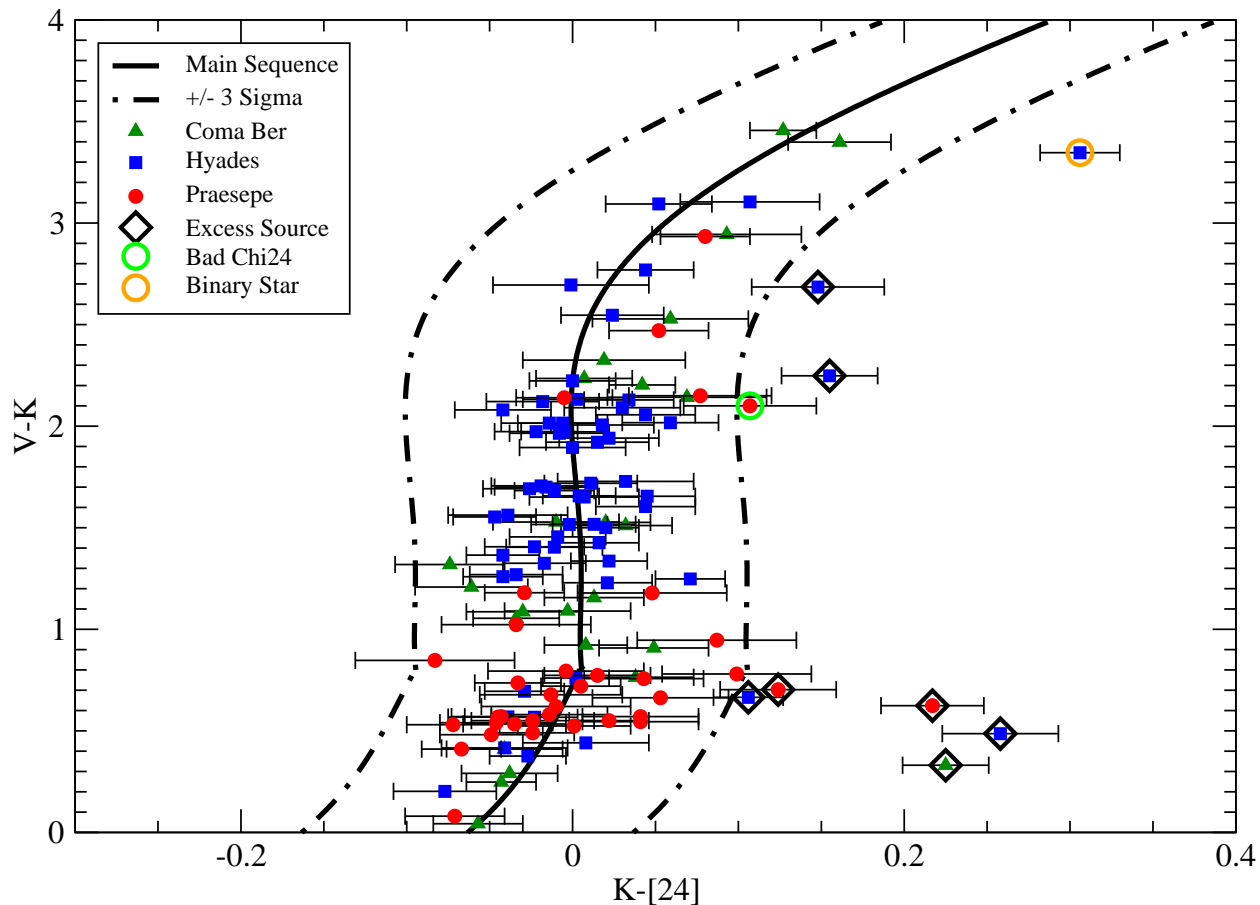


Fig. 3.—  $V - K_S$  vs.  $K_S - [24]$  color-color plot for 670 Myr cluster members that we retain in our analysis. The solid line is the locus of main sequence stars and the dash-dot lines are at  $3\sigma$  above and below in  $K_S - [24]$ . The stars that pass our tests for having  $24 \mu\text{m}$  excesses are indicated with diamonds. One additional star circled in green, 2MASSJ08385506+1911539, lies to the right of the  $3\sigma$  locus but fails our signal-to-noise criterion for a verified excess, as can also be seen by the large error bars for it (Section 3.1). HIP21179 is circled in orange because of a possible false excess due to a binary companion (Section 3.3).